Frequency Division Multiplexed Radio-over-Fiber Transmission using an Optically Injected Laser Diode

Sze-Chun Chan
Department of Electronic Engineering, City University of Hong Kong, Hong Kong, China

ABSTRACT

Nonlinear dynamics of semiconductor lasers have recently attracted much attention in the area of microwave photonics. By invoking the nonlinear dynamics of an optically injected laser diode, high-speed microwave oscillation can be generated using the period-one oscillation state. The oscillation is harnessed for application as a photonic microwave source in radio-over-fiber (RoF) systems. It is advantageous over conventional direct current modulation because it alleviates the modulation bandwidth limitation and naturally generates single sideband signals. The method is thus applicable to wireless communication systems even when the subcarrier frequency increases to 60 GHz. Because RoF is usually incorporated with standard wireless schemes that involve frequency division multiplexing (FDM), we investigate the performance of the optical injection system under simultaneous current injection of multiple data streams. Frequency mixings and competition for locking among subcarriers result in intermodulation distortion (IMD). The relative weightings of different channels should be optimized to ensure acceptable signal qualities. The results illustrate the feasibility of applying the optical injection system for FDM RoF transmission at high subcarrier frequencies.

Keywords: Nonlinear dynamics, optical injection, frequency division multiplexing (FDM), radio-over-fiber (RoF), microwave photonics

1. INTRODUCTION

Radio-over-fiber (RoF) technology has gained much importance as a cost-effective wireless solution. Optical fiber transmission of microwave allows deployment of large number of radio access points. Each access point contains simply a photodetector, an microwave amplifier, and an antenna while the expensive high-speed electronics are centralized in the central office. In the near future, the microwave subcarrier frequency will be designed in the 60-GHz band, where about 7 GHz of unlicensed bandwidth is available.[1] Some other important frequencies are also included in the IEEE 802 standards for wireless links. Potential RoF photonic microwave sources include the optoelectronic oscillator (OEO), two-laser beating, electro-optic modulators, external cavity semiconductor lasers, and multi-section semiconductor lasers. [2-7] In this paper, we focus on an RoF source based on the nonlinear dynamics of optically injected semiconductor lasers,[8] which is a simple solution for widely tunable RoF generation.

Properly adjusted injection undamps the relaxation oscillation and generates a widely tunable microwave oscillation known as the period-one oscillation. The oscillation can be tuned beyond the original bandwidth of the laser for 60 GHz applications. Since most RoF wireless applications employ frequency division multiplexing (FDM), it is interesting to investigate the performance of the system when multiple subcarriers are used. The effects of intermodulation distortion (IMD) that cause signal degradation should be minimized. Kaszubowska et al. have previously demonstrated multiplexed transmission of a similar system at a lower frequency.[2] It was found that unequally spaced channels are advantageous over equally spaced channels in IMD performances. However, equally spaced channels are still of practical importance. It is interesting to examine the effects of IMD for equally spaced channels.

In this paper, simultaneous transmission of 4 channels at around 60-GHz is investigated based on the well established rate equation model. It is found that frequency mixings and competition for locking among subcarriers both contribute to IMD. The relative weightings of different channels should be optimized to ensure acceptable signal qualities. Following this introduction, the setup under consideration is presented in Section 2. The FDM downlink is then reported in Section 3. Detailed investigations on the IMD are presented in Section 4. It is followed by a conclusion in Section 5.

*scchan@cityu.edu.hk; phone (852) 2784-4227

Semiconductor Lasers and Laser Dynamics III, edited by Krassimir P. Panayotov, Marc Sciamanna, Angel A. Valle, Rainer Michalzik, Proc. of SPIE Vol. 6997, 69971Y, (2008) · 0277-786X/08/$18 · doi: 10.1117/12.781638

2. SETUP

The schematic of the setup under consideration is shown in Fig. 1. The central part of the setup is an optical injection system consisting of a master laser (ML) and a slave laser (SL). Light is injected from the master laser to the slave laser unidirectionally through an optical isolator (OI). The normalized injection strength ξ_{inj} and the frequency detuning f_{inj} between the two lasers can be varied. The detuning is defined as the optical frequency difference of the master laser from the slave laser under the free-running condition. By properly adjusting these injection parameters, the slave laser is first injection-locked by the master laser and then enters the nonlinear dynamical period-one oscillation state. Its output intensity thus oscillates at a microwave frequency f_0. The frequency is widely tunable. Although the slave laser has a relaxation frequency of 10 GHz, f_0 can be tuned to 60 GHz for RoF applications. The oscillation is generated even without applying any current modulation on the slave laser. However, the oscillation can be easily locked when an external microwave current is applied. Light is transmitted over fiber and is detected by a photodiode (PD). The microwave signal f_0 is extracted from the optical carrier by the photodiode and is subsequently transmitted over a microwave link. The microwave link can be a wireless link in practical systems, but the details of the microwave propagation are omitted here.

FDM data modulation is achieved with binary phase-shift keying (BPSK). We consider 4 channels of baseband data $d_i(t)$ for i = 1, 2, 3, and 4. The data rate is 51.84 Mbps for each channel. Using electrical mixers, the data streams are upconverted to 4 equally separated microwave subcarriers f_1 = 59.68896 GHz, f_2 = 59.89632 GHz, f_3 = 60.10368 GHz, and f_4 = 60.31104 GHz. In order to minimize cross-talk, each channel is sent to a corresponding bandpass filter (BPF) with a bandwidth of 207.36 MHz. The amplitude of each channel can be independently controlled by a weighting factor w_i. The filtered signals are then combined into the multiplexed signal $m(t)$. This electrical signal is around 60 GHz and is thus capable of locking the original period-one oscillation. Therefore, the output of the slave laser is forced to carry the FDM data. The signal is sent over fiber to a photodiode at an access point.

After the photodiode, the FDM signal can be radiated to the wireless units. Upon receiving the microwave signal, demodulation is achieved by first splitting the signal into 4 demodulation channels. For each channel i, the signal is downconverted by electrically mixing with a local oscillator at f_i. The downconverted signals are then sent through lowpass filters (LPF) that have a cutoff frequency at 103.68 MHz. The outputs are the recovered data signals $\tilde{d}_i(t)$ for i = 1, 2, 3, and 4. The local oscillators are assumed to be properly phase-locked, which can be achieved using phase-lock loop circuits in typical wireless systems.

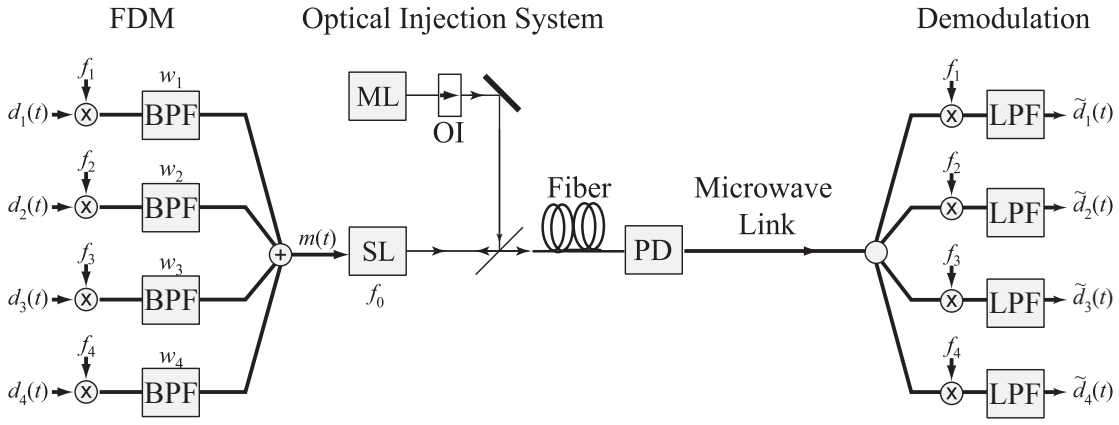

Fig. 1. Schematic of using the optical injection system under period-one oscillation at f_0 for FDM RoF transmission. ML: master laser; SL: slave laser; OI: optical isolator; PD: photodiode; BPF: bandpass filter; and LPF: lowpass filter. For each channel i, binary data $d_i(t)$ are upconverted to a subcarrier f_i and weighted by a constant factor w_i, where i = 1, 2, 3, and 4. The frequency of the multiplexed signal $m(t)$ is near the original period-one oscillation frequency f_0. It is used to injection-lock and modulate the oscillation. After the fiber, the photodiode at the access point extracts the microwave signal. Demodulation is achieved by downconversion of the microwave signal to the baseband data $\tilde{d}_i(t)$.

The dynamics of the optical injection system is described by the following rate equation model:[9]

$$\frac{da_r}{dt} = \frac{1}{2}\left[\frac{\gamma_c\gamma_n}{\gamma_s\tilde{J}}\tilde{n} - \gamma_p(a_r^2 + a_i^2 - 1)\right](a_r + ba_i) + \xi_{inj}\gamma_c \cos 2\pi f_{inj}t \tag{1}$$

$$\frac{da_i}{dt} = \frac{1}{2}\left[\frac{\gamma_c\gamma_n}{\gamma_s\tilde{J}}\tilde{n} - \gamma_p(a_r^2 + a_i^2 - 1)\right](-ba_r + a_i) - \xi_{inj}\gamma_c \sin 2\pi f_{inj}t \tag{2}$$

$$\frac{d\tilde{n}}{dt} = -\left[\gamma_s + \gamma_n(a_r^2 + a_i^2)\right]\tilde{n} - \gamma_s\tilde{J}(a_r^2 + a_i^2 - 1) + \frac{\gamma_s\gamma_p}{\gamma_c}\tilde{J}(a_r^2 + a_i^2)(a_r^2 + a_i^2 - 1) + \alpha m(t)\gamma_s(1 + \tilde{J}) \tag{3}$$

where a_r and a_i respectively are the real and imaginary parts of normalized complex intracavity field amplitude at the free-running slave laser frequency, $1 + \tilde{n}$ is the normalized charge carrier density, $\tilde{J}$ is the normalized bias current above the threshold, ξ_{inj} is the dimensionless injection strength, f_{inj} is the injection detuning as defined before, γ_c is the cavity decay rate, γ_s is the spontaneous carrier relaxation rate, γ_n is the differential carrier relaxation rate, γ_p is the nonlinear carrier relaxation rate, and b is the linewidth enhancement factor. The following parameter values are adopted: $\gamma_c = 5.36\times10^{11}(s^{-1})$, $\gamma_s = 5.96\times10^{9}(s^{-1})$, $\gamma_n = 7.53\times10^{9}(s^{-1})$, $\gamma_p = 2.34\times10^{10}$ (s^{-1}), $b = 3.2$, and $\tilde{J} = 1.222$. With these parameters, the relaxation resonance frequency of the slave laser is about 10 GHz. Data modulation from the FDM signal $m(t)$ is included by the last term of Eq. (3), where α is the data modulation depth. High-order effects of the current modulation are neglected.

Figure 2 shows the period-one oscillation state generated by the optical injection. The injection strength is set at $\xi_{inj} = 0.447$ and the detuning is set at $f_{inj} = 55$ GHz. The optical spectra are offset to the free-running frequency of the slave laser. In Fig. 2(a), the spectrum is obtained without any current modulation when $\alpha = 0$. Injection from the master laser is indicated by the arrow. Period-one oscillation at $f_0 = 60$ GHz is generated such that the spectrum consists of mainly two optical lines of nearly equal amplitudes. The high-speed oscillation is not possible without the optical injection. In Fig. 2(b), the spectrum is obtained when data modulation with $\alpha = 0.5$ is applied. All channels are equally weighted by setting $(w_1, w_2, w_3, w_4) = (1, 1, 1, 1)$. The modulation can be regarded as a microwave injection that locks the original period-one oscillation. The original oscillation at frequency f_0 disappears and is replaced by the components at f_1, f_2, f_3, and f_4. Data are imposed through the locking. The optical spectrum shows the resultant data sidebands. The technique is applicable to a wide range of subcarrier frequencies as long as the original frequency f_0 is first properly tuned to the proximity of the desired subcarrier frequencies. The tuning is shown in Fig. 2(c) as a function of the required injection strength ξ_{inj}. The injection detuning f_{inj} is kept constant and $\alpha = 0$ in this plot. The corresponding microwave power generated through beating at the photodiode is also shown. It shows that the period-one oscillation can be tuned and the associated microwave power remains nearly constant. For a typical photodiode of 0.5-A/W sensitivity and using a modest optical power of 1 mW, the microwave power generated is about −25 dBm, which can be easily amplified at the access points. It should also be mentioned that the optical spectrum is asymmetric, which is advantageous for low power penalty RoF transmission.[9-10]

3. FDM DOWNLINK

In the following simulations, the optical injection conditions are kept at $\xi_{inj} = 0.447$ and $f_{inj} = 55$ GHz. The generated period-one oscillation frequency is $f_0 = 60$ GHz. Figure 3 shows the power spectrum at the photodiode and the recovered data signals when the input data modulation depth is $\alpha = 0.5$. The weightings of the different component channels are adjusted.

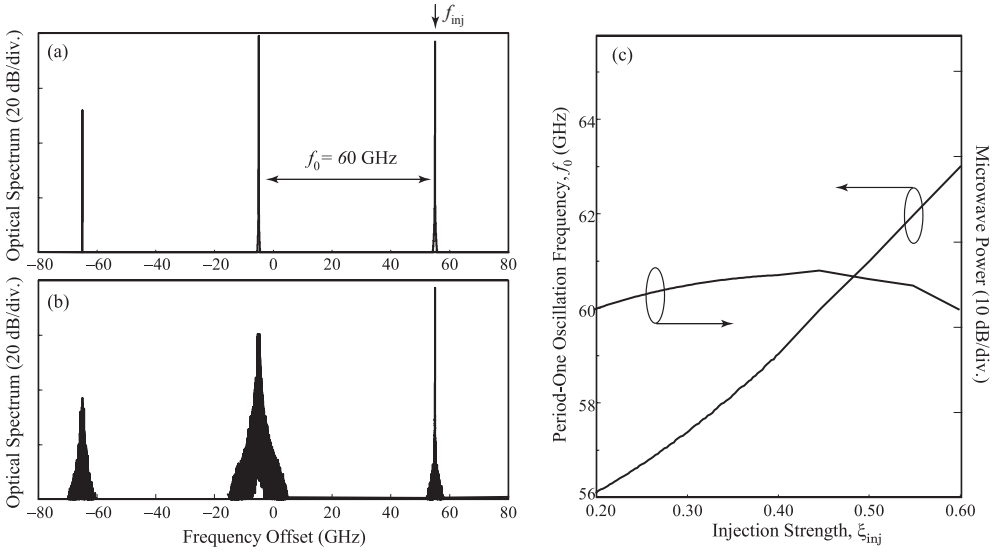

Fig. 2. Period-one oscillation state under optical injection at a detuning of f_{inj} = 55 GHz (as indicated by the arrow). (a) Optical spectrum of the slave laser under period-one oscillation at f_0 = 60 GHz without any current modulation. The frequency axis is offset to the free-running optical frequency of the slave laser. (b) Optical spectrum obtained when the bias current is modulated with the data signal $m(t)$. (c) Period-one oscillation frequency as a function of the injection strength ξ_{inj}. The corresponding microwave power is obtained after optoelectronic conversion by the photodiode.

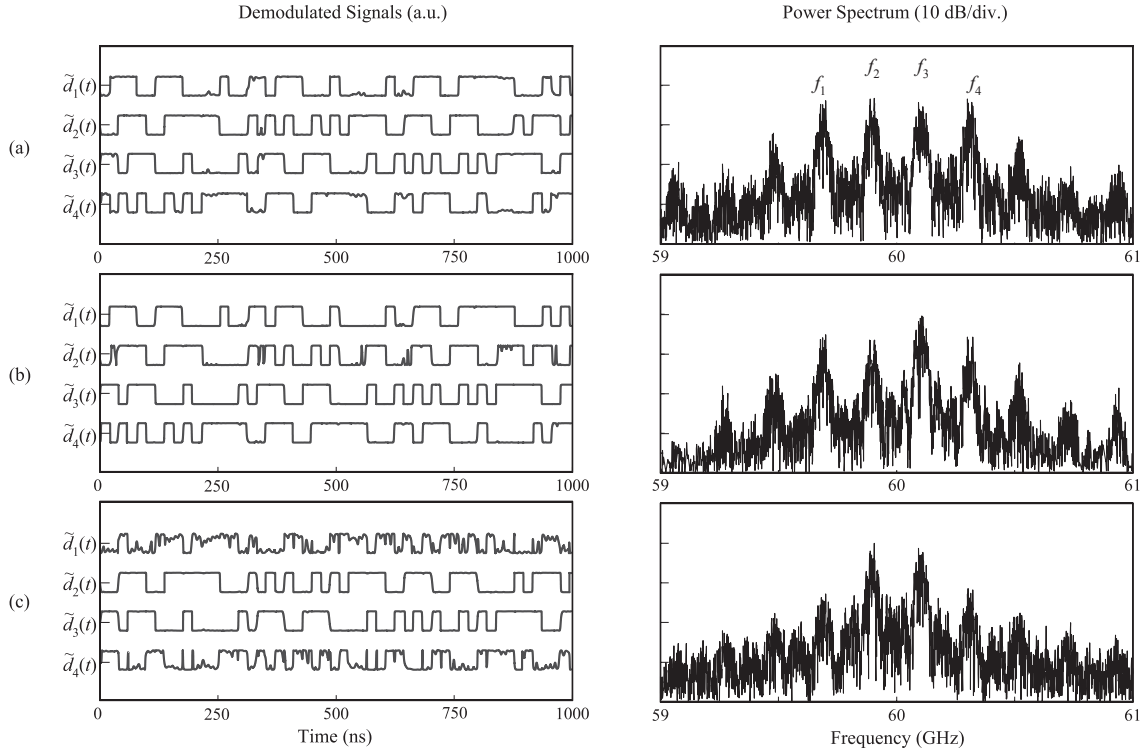

Fig. 3. Power spectrum obtained at the photodiode and the demodulated signals $\tilde{d}_i(t)$ for i =1, 2, 3 and 4. The data modulation depth α is kept constant at 0.5. The component weightings (w_1, w_2, w_3, w_4) are: (a) (1, 1, 1, 1), (b) (1, 1, 2, 1), and (c) (0, 1, 1, 0).

In Fig. 3(a), the weightings are set as (w_1, w_2, w_3, w_4) = (1, 1, 1, 1). The equally weighted channels clearly give their peaks at f_1, f_2, f_3, and f_4. The corresponding time traces also show good recovery of the data signals as $\tilde{d}_1(t)$, $\tilde{d}_2(t)$, $\tilde{d}_3(t)$, and $\tilde{d}_4(t)$, respectively. The recovered signal quality is measured to be Q = 4.5 and it can be improved by employing better bandpass and lowpass data filters. In Fig. 3(b), the weightings are changed to (w_1, w_2, w_3, w_4) = (1, 1, 2, 1). Because the component at f_3 is strengthened, the period-one oscillation is under strong influence of this component and so the adjacent channels are affected. The power spectrum shows that the peak at f_3 is increased while the peak at f_2 is suppressed in magnitude. Thus, the locking of the period-one oscillation to f_3 causes a degradation of $\tilde{d}_2(t)$, which is shown on the corresponding time trace. Channel 4 is affected similarly, but the effect is relatively weak. In Fig. 3(c), the weightings are changed to (w_1, w_2, w_3, w_4) = (0, 1, 1, 0). Although Channels 1 and 4 are switched off, the power spectrum still shows the frequency components at f_1 and f_4. They are due to the frequency mixings between the components f_2 and f_3. The residual time traces of $\tilde{d}_1(t)$ and $\tilde{d}_4(t)$ do not represent true data of Channels 1 and 4. Therefore, both the competition of locking and the microwave frequency mixings contribute to IMD of the optical injection system.

The quality of a data stream can be quantified by the Q of the corresponding time trace, which can be converted into dB scale as $20\log_{10}Q$. Figure 4 shows the values of Q as the modulation depth α varies. The weightings are kept equal as (w_1, w_2, w_3, w_4) = (1, 1, 1, 1). The circles, triangles, squares, and diamonds correspond to Channels 1, 2, 3, and 4, respectively. The closed symbols show the qualities of the recovered signals $\tilde{d}_1(t)$, $\tilde{d}_2(t)$, $\tilde{d}_3(t)$, and $\tilde{d}_4(t)$. It is observed that the curves start to saturate at about α = 0.5. The data modulation is strong enough to lock the period-one modulation. Channel 3 is locked the best because it is closest to the original 60 GHz oscillation. Channel 1 is locked the worst in this case. Locking is typically biased towards the positively detuned frequencies, which was also observed in related systems.[11] As a reference, the open symbols show the signal qualities obtained when the optical part is bypassed. They are measured by sending the electrical message $m(t)$ directly for demodulation. The measured signal qualities are not perfect because the filters limit the data bandwidths.

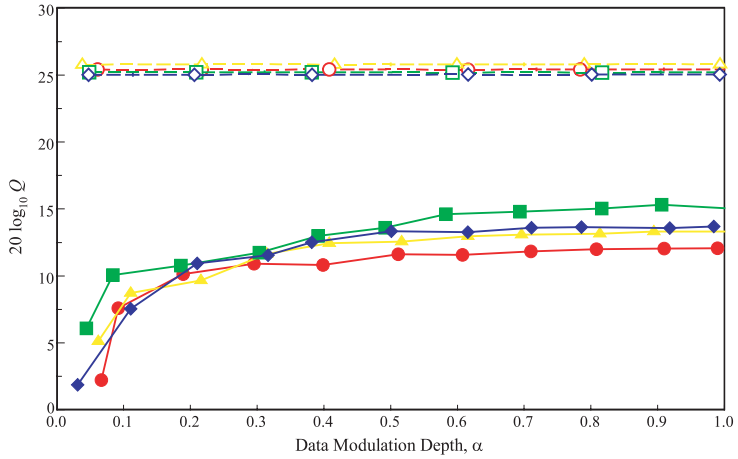

Fig. 4. Signal qualities Q of the demodulated signals (closed symbols) versus the data modulation depth α. The input signal qualities are also shown (open symbols) for comparison. The circles, triangles, squares, and diamonds correspond to Channels 1, 2, 3, and 4, respectively.

4. EFFECTS OF INTERMODULATION DISTORTION (IMD)

In the following, α is kept constant at 0.5 while the weightings of the channels are varied separately. The effect of IMD manifests as variations of Q in Fig. 5. The open symbols and the closed symbols again correspond to the reference and the recovered data, respectively. Also, the circles, triangles, squares, and diamonds correspond to Channels 1, 2, 3, and 4, respectively.

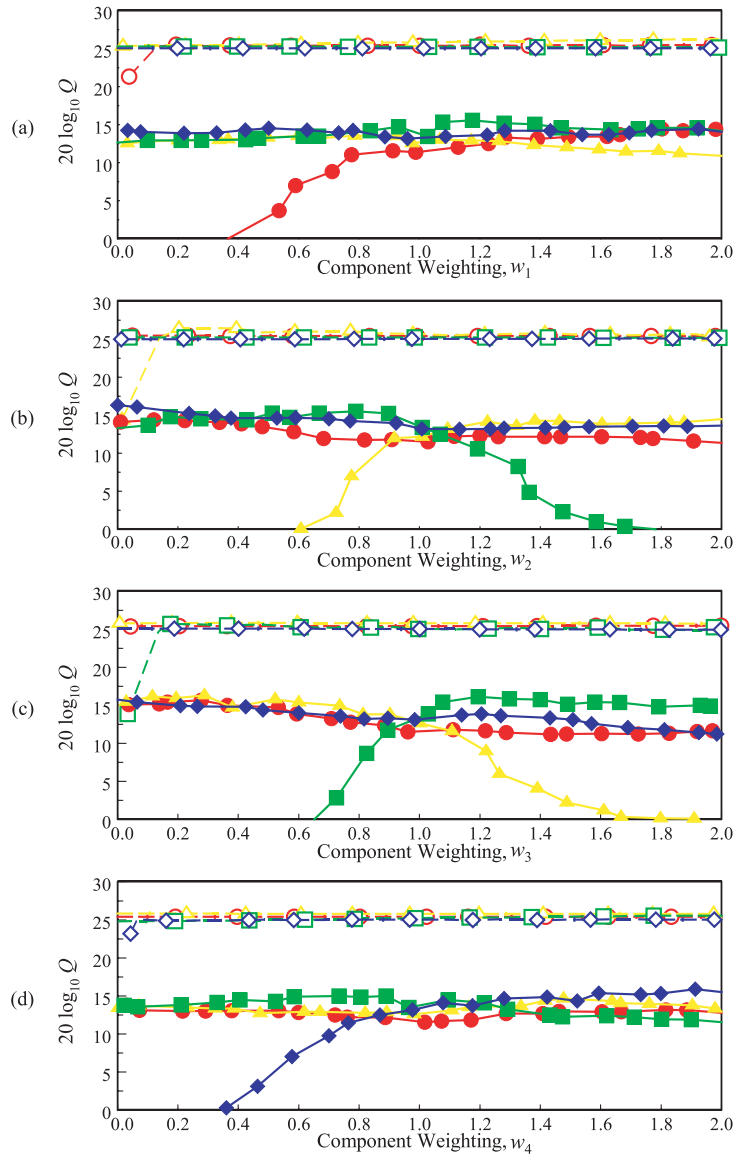

Fig. 5. Variations of the signal qualities Q when different component weightings are varied. Weightings w_1, w_2, w_3, and w_4 are varied in (a), (b), (c), and (d), respectively. In each plot, the remaining weightings are kept at 1. Signal qualities Q of the recovered signals are shown as closed symbols while that of the corresponding input signals are shown in open symbols. The circles, triangles, squares, and diamonds correspond to Channels 1, 2, 3, and 4, respectively.

In Fig. 5(a), w_1 is varied while w_2, w_3, and w_4 are kept constant at 1. It is observed that Q of Channel 1 increases with w_1. The rest of the channels only degrade slightly as w_1 increases. In Fig. 5(b), w_2 is varied while w_1, w_3, and w_4 are kept constant at 1. The quality of Channel 2 increases with w_2 as expected, but at the same time it competes with Channel 3 for locking. Channel 3 thus shows significant degradation as w_2 increases. The reverse occurs in Fig. 5(c) when w_3 is varied instead. Here, Channel 3 improves and Channel 2 degrades as w_3 increases. In Fig. 5(d), w_4 is varied while w_1, w_2, and w_3 are kept constant at 1. Channel 4 shows improvements as w_4 increases, but the rest of the channels only degrade slightly. Therefore, we observe that the strongest interaction takes place between Channels 2 and 3. They are both closest to the original period-one oscillation at 60 GHz. Their mutual influences can be understood as competitions for locking of the period-one oscillation.

According to Fig. 5, the effects of IMD are the strongest for Channels 2 and 3. The signal qualities are examined in Fig. 6 as both w_2 and w_3 are varied. The qualities of Channels 1, 2, 3, and 4 are shown as Q_1, Q_2, Q_3, and Q_4, respectively. In each plot, w_3 is continuously varied while different values of w_2 are used for different curves. The values of w_2 are 0.1, 0.5, 1.0, 1.2, 1.5, and 2.0 for closed circles, closed triangles, closed squares, open circles, open triangles, and open squares, respectively. The other two weightings are kept constant as $w_1 = w_4 = 1$. Figures 6(b) and (c) clearly show the competition between Channels 2 and 3. For each value of w_2, Channel 2 has a better quality than Channel 3 when $w_2 > w_3$. The opposite is true when $w_2 < w_3$. The changes of signal qualities are significant. For example, the curve for $w_2 = 0.5$ in Fig. 6(b) shows that the quality of Channel 2 is degraded by about 17 dB as w_3 increases from 0 to 2. By contrast, the family of curves of Figs. 6(a) and (b) show less pronounced IMD effects. The degradations due to w_3 are always less than 8 dB according to the plots. In any case, the signal qualities decrease as w_2 or w_3 increases.

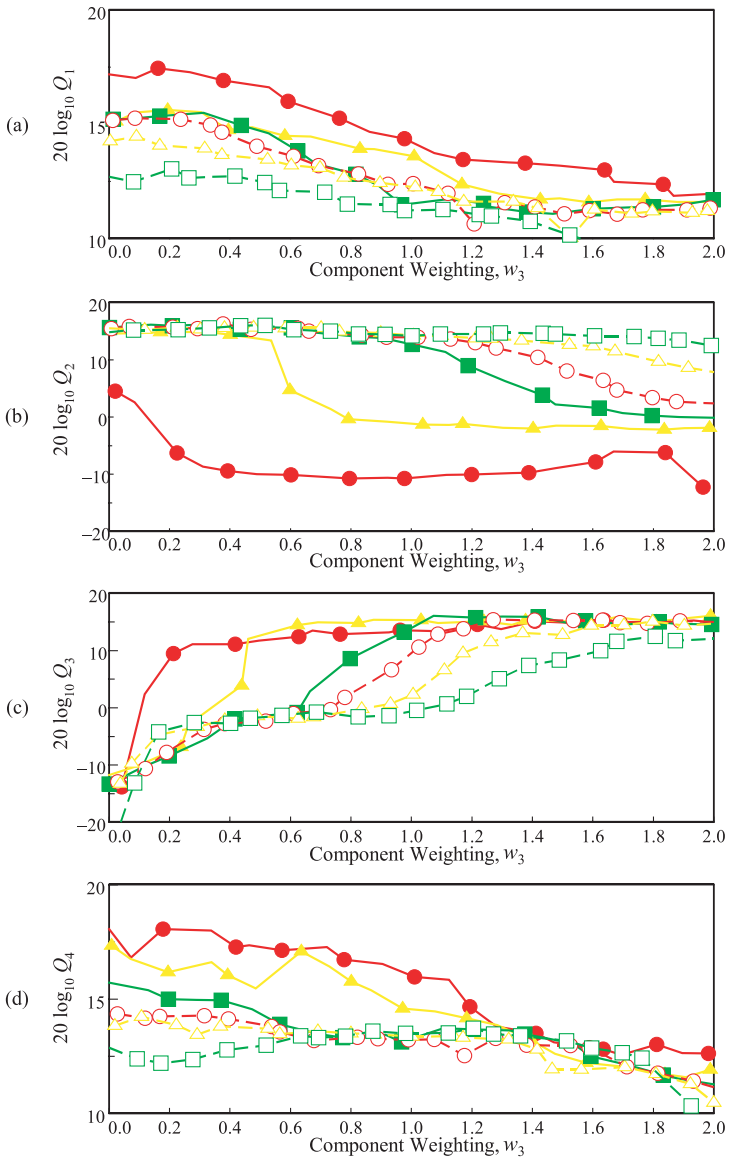

Fig. 6. Variations of the signal qualities Q_i for Channels i = 1, 2, 3, and 4 as the weightings w_3 and w_2 are varied. The channels are plotted separately: (a) Channel 1, (b) Channel 2, (c) Channel 3, and (d) Channel 4. Closed circles, closed triangles, closed squares, open circles, open triangles, and open squares correspond to w_2 = 0.1, 0.5, 1.0, 1.2, 1.5, and 2.0, respectively. The weightings for the other two channels are kept constant as $w_1 = w_4 = 1$.

For completeness, the IMD effects are also investigated when both w_4 and w_3 are varied. The results are shown in Figs. 7(a) to (d). In each plot, w_3 is continuously varied while different values of w_4 are used for different curves. The values of w_4 are 0.1, 0.5, 1.0, 1.2, 1.5, and 2.0 for the closed circles, closed triangles, closed squares, open circles, open triangles, and open squares, respectively. The other two weightings are kept constant at 1. In Fig. 7(d), the family of curves shows that Q_4 increases as w_4 increases. The improvement is stopped for values of w_4 greater than 1.0. Similarly, Fig. 7(c) shows that Q_3 increases as w_3 increases. It is not much affected by w_4 for w_3 >1.0.

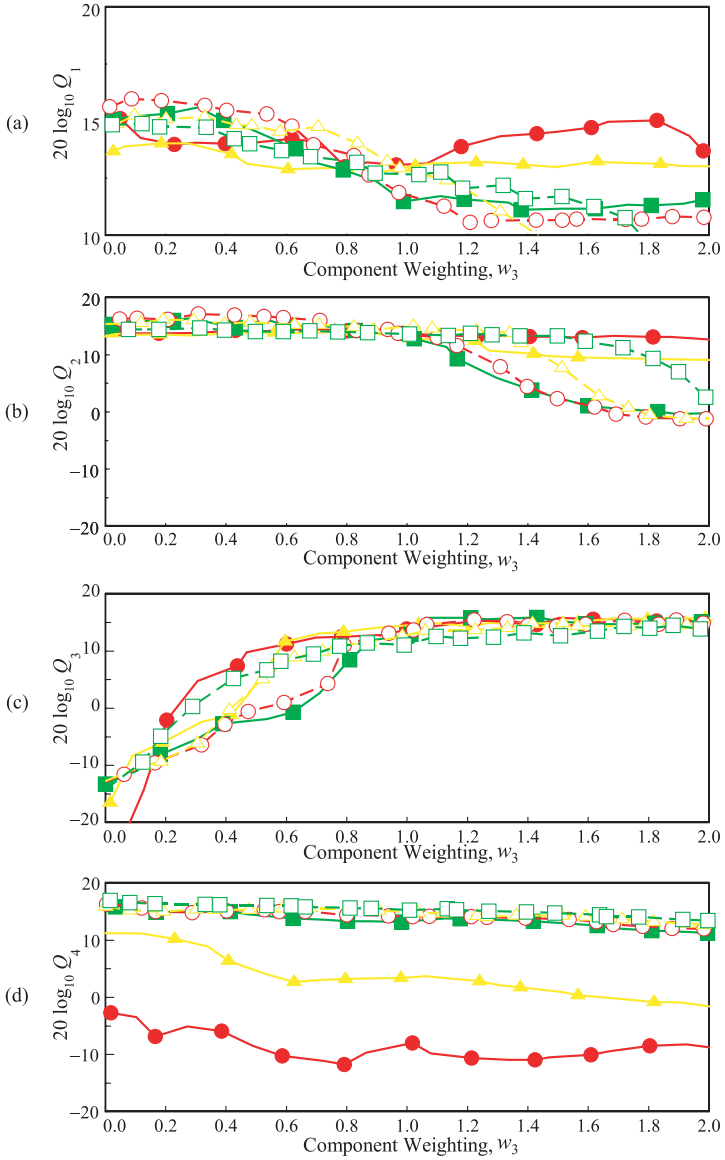

Fig. 7. Variations of the signal qualities Q_i for Channels i = 1, 2, 3, and 4 as the weightings w_3 and w_4 are varied . The channels are plotted separately: (a) Channel 1, (b) Channel 2, (c) Channel 3, and (d) Channel 4. Closed circles, closed triangles, closed squares, open circles, open triangles, and open squares correspond to w_4 = 0.1, 0.5, 1.0, 1.2, 1.5, and 2.0, respectively. The weightings for the other two channels are kept constant as $w_1 = w_2 = 1$.

In Fig. 7(b), it is observed that Q_2 is degraded when w_3 is increased above 1.0. For w_4 = 0.1, 0.5, and 1.0, the corresponding power spectra reveal that f_3 is the strongest component. Thus, as w_4 increases, frequency mixings between f_3 and f_4 degrade the quality of Channel 2. However, for w_4 = 1.2, 1.5, and 2.0, the corresponding power spectra reveal that f_4 becomes the strongest component. The component at f_3 is weakened and thus the quality of f_2 increases with w_4. Figure 7(a) shows a similar, but less pronounced, behavior for the signal quality of Channel 1. The above results show that the effect of IMD depends on the relative weightings of the channels. The channels should be well balanced to mitigate the effects.

5. CONCLUSION

In summary, FDM RoF application of the nonlinear dynamics of optically injected semiconductor lasers is investigated numerically. Period-one oscillation at 60 GHz is generated by the optical injection alone and the oscillation is subsequently modulated by an FDM signal. Due to the frequency mixings and competition for locking among FDM subcarriers, IMD degradations are observed in recovered data signals. In the future, signals of wider bandwidth can be examined and experiments can be conducted for detailed investigation of the IMD effects.[12]

ACKNOWLEDGMENTS

The author is grateful to the support of the City University of Hong Kong under project no. 7200110.

REFERENCES

1. P. Smulders, H. Yang, and I. Akkermans, “On the design of low-cost 60-GHz radios for multigigabit-per-second transmission over short distances”, *IEEE Commun. Magn.* 45, 44-51 (2007).
2. A. Kaszubowska, L. P. Barry, and P. Anandarajah, “Effects of intermodulation distortion on the performance of a hybrid radio/fiber system employing a self-pulsating laser diode transmitter,” *IEEE Photon. Technol. Lett.* 15, 852-854 (2003).
3. T. B. Simpson and F. Doft, “Double-locked laser diode for microwave photonics applications,” *IEEE Photon. Technol. Lett.* 11, 1476-1478 (1999).
4. B. L. Dang, M. G. Larrode, R. V. Prasad, I. Niemegeers, and A. M. J. Koonen, “Radio-over-fiber based architecture for seamless wireless indoor communication in the 60 GHz band”, *Computer Commun.* 30, 3598-3613 (2007).
5. A. Martinez, V. Polo, J. L. Corral, and J. Marti, “Experimental demonstration of dispersion-tolerant 155-Mb/s BPSK data transmission at 40 GHz using an optical coherent harmonic generation technique", *IEEE Photon. Technol. Lett.* 15, 772-774 (2003).
6. K. Kojucharow, M. Sauer, H. Kaluzni, D. Sommer, F. Poegel, W. Nowak, A. Finger, and D. Ferling, “Simultaneous electrooptical upconversion, remote oscillator generation, and air transmission of multiple optical WDM channels for a 60-GHz high-capacity indoor system", *IEEE Trans. Microwave Theory Tech.* 47, 2249-2256 (1999).
7. C. Lim, A. Nirmalathas, and D. Novak, “Techniques for multichannel data transmission using a multisection laser in millimeter-wave fiber-radio systems”, *IEEE Trans. Microwave Theory Tech.* 47, 1351-1357 (1999).
8. S. C. Chan and J. M. Liu, “Tunable narrow-linewidth photonic microwave generation using semiconductor laser dynamics,” *IEEE J. Select. Topics Quantum Electron.* 10, 1025-1032 (2004).
9. S. C. Chan, S. K. Hwang, and J. M. Liu, “Period-one oscillation for photonic microwave transmission using an optically injected semiconductor laser”, *Opt. Express* 15, 14921-14935 (2007).
10. H. S. Ryu, Y. K. Seo, and W. Y. Choi, “Dispersion-tolerant transmission of 155-Mb/s data at 17 GHz using a 2.5-Gb/s-grade DFB laser with wavelength-selective gain from an FP laser diode,” *IEEE Photon. Technol. Lett.* 16, 1942-1944 (2004).
11. S. C. Chan and J. M. Liu, “Microwave frequency division and multiplication using an optically injected semiconductor laser”, *IEEE J. Quantum Electron.* 41, 1142-1147 (2005).
12. S. C. Chan, S. K. Hwang, and J. M. Liu, “Radio-over-fiber AM-to-FM upconversion using an optically injected semiconductor laser,” *Opt. Lett.* 31, 2254-2256 (2006).